MOLECULAR AND CELLULAR BIOLOGY, July 2006, p. 5394–5405 Vol. 26, No. 14
0270-7306/06/$08.00+0 doi:10.1128/MCB.00519-06

The X and Y Chromosomes Assemble into H2A.Z, Containing Facultative Heterochromatin, following Meiosis

Ian K. Greaves,[1] Danny Rangasamy,[1] Michael Devoy,[1] Jennifer A. Marshall Graves,[2] and David J. Tremethick[1]*

The John Curtin School of Medical Research, The Australian National University, P.O. Box 334, Canberra, Australian Capital Territory, 2601 Australia,[1] and Comparative Genomics Group, Research School of Biological Sciences, The Australian National University, Canberra, Australian Capital Territory, 2601 Australia[2]

Received 24 March 2006/Accepted 13 April 2006

Spermatogenesis is a complex sequential process that converts mitotically dividing spermatogonia stem cells into differentiated haploid spermatozoa. Not surprisingly, this process involves dramatic nuclear and chromatin restructuring events, but the nature of these changes are poorly understood. Here, we linked the appearance and nuclear localization of the essential histone variant H2A.Z with key steps during mouse spermatogenesis. H2A.Z cannot be detected during the early stages of spermatogenesis, when the bulk of X-linked genes are transcribed, but its expression begins to increase at pachytene, when meiotic sex chromosome inactivation (MSCI) occurs, peaking at the round spermatid stage. Strikingly, when H2A.Z is present, there is a dynamic nuclear relocalization of heterochromatic marks (HP1β and H3 di- and tri-methyl K9), which become concentrated at chromocenters and the inactive XY body, implying that H2A.Z may substitute for the function of these marks in euchromatin. We also show that the X and the Y chromosome are assembled into facultative heterochromatic structures postmeiotically that are enriched with H2A.Z, thereby replacing macroH2A. This indicates that XY silencing continues following MSCI. These results provide new insights into the large-scale changes in the composition and organization of chromatin associated with spermatogenesis and argue that H2A.Z has a unique role in maintaining sex chromosomes in a repressed state.

At the most basic level, the mammalian genome is partitioned into domains that are compacted and repressed (heterochromatin) or less condensed and gene rich (euchromatin). However, more complex levels of chromatin organization exist. For example, heterochromatin can be further classified as constitutive or facultative.

In all higher eukaryotes, constitutive heterochromatic structures are assembled at the ends of chromosomes and at the centromere (pericentric heterochromatin) to maintain these important functional domains in a stable state. Rather than being structurally static as first believed, it is becoming clear that these large highly compacted domains are dynamic since their protein composition can change during cellular differentiation (10, 26, 50), between transitions from proliferation to quiescence (21), and when the levels of CpG methylation are altered (37). This argues that the function(s) of constitutive heterochromatin may vary with the cellular context. For example, during the differentiation of extraembryonic lineages in preimplanation mouse embryos, H2A.Z becomes enriched at pericentric heterochromatin (50). MacroH2A then relocates from pericentric heterochromatin to the inactive X chromosome to silence gene expression (10). These two variants do not appear to coexist at the same place, suggesting that they have distinct functions within the context of heterochromatin (50).

Mice deficient in H2A.Z die early in development around the time of implantation (13). Our recent studies suggest that this essential function of H2A.Z may relate to its role in the chromosome segregation process (51). Using a variety of mammalian cell lines, we have shown that, whereas H2A.Z is a minor component of pericentric heterochromatin compared to H2A (and thus difficult to detect by indirect immunofluorescence), it has a major structural role in maintaining the integrity of pericentric heterochromatin and, without it, sister chromatid cohesion is lost (I. Greaves and D. Tremethick, unpublished data), leading to defects in chromosome segregation (51). The concentration of H2A.Z in constitutive heterochromatin can vary depending on the differentiation state (50). Consistent with this function, recent biophysical studies of nucleosomal arrays have shown that H2A.Z, compared to H2A, can generate condensed chromatin secondary structures (14), and this level of compaction is enhanced with HP1α (15). Interestingly, ARP 6, a unique component of the SWR1 complex, which has been proposed to deposit H2A.Z at specific chromatin loci (31, 32, 42), is required for telomeric silencing in fission yeast (64).

In addition to H2A.Z having a role in maintaining large chromosomal domains, H2A.Z may also function at a local level. Recent studies in budding yeast have shown that H2A.Z is associated with a small number of nucleosomes at inactive promoters, but these H2A.Z containing nucleosomes are displaced upon gene activation. Since these H2A.Z-containing nucleosomes are specifically positioned and inhibit histone modifiers associated with transcription (35), they may contribute to the unique architecture of a promoter poised to be activated (22, 35, 49, 67). H2A.Z found at promoters or at

* Corresponding author. Mailing address: The John Curtin School of Medical Research, The Australian National University, P.O. Box 334, Canberra, Australian Capital Territory, 2601 Australia. Phone: 61261252326. Fax: 61261250415. E-mail: david.tremethick@anu.edu.au.

condensed chromatin may be distinguished by its acetylation state (3). It is worth noting that the amino acid sequence of budding yeast H2A.Z compared to mouse H2A.Z differ significantly at the N and C termini (55).

It has been proposed that histone posttranslational modifications also play an important role in the formation of constitutive heterochromatin. Mouse pericentric heterochromatin is enriched with H3-K9 trimethylation, H3-K27 monomethylation, and H4-K20 trimethylation (33). Consistent with the plasticity of this heterochromatic domain, loss of the *Suv39h* histone methyltransferase (required for H3-K9 trimethylation) changes the methylation pattern as pericentric heterochromatin accumulates H3-K27 trimethylation and K9 monomethylation (46).

The formation of facultative heterochromatin is developmentally regulated (17). Most of the genome, which contains genes not needed for a specific cell lineage pathway, is silenced by the assembly into compacted domains of facultative heterochromatin (17). The dynamic nature of this type of heterochromatin enables it to return to a transcriptionally activated state (5, 12, 23). Mouse facultative heterochromatin is defined by a different set of histone posttranslational modifications, H3-K9 dimethylation and H3-K27 trimethylation (46, 53). macroH2A can participate in the formation of both facultative and constitutive heterochromatin (9, 10, 26) (see below).

The mechanisms that partition the genome into these different heterochromatic states are poorly understood. Given the major chromosome reorganization events and associated compositional and histone modification changes, mouse spermatogenesis provides a unique opportunity to study the establishment of distinct structural and functional chromatin states. Mammalian spermatogenesis is a complex process involving the differentiation of diploid and then haploid germ cells (44). Of particular importance is the process of meiotic sex chromosome inactivation (MSCI), an evolutionarily driven process in which both the X and the Y chromosome become heterochromatic and transcriptionally inactive during meiotic prophase I at pachytene (29, 52).

A wide variety of histone modifications and histone variants (ubiquitous and testes specific) have been identified at distinct stages throughout spermatogenesis (7, 8, 19, 24, 34). Phosphorylated H2A.X (16, 60) and macroH2A1.2 (26, 27, 54, 57) participate in the assembly of the X and Y chromosomes into facultative heterochromatin at the onset of MSCI but are removed at later stages. In mature sperm, macroH2A1.2 can no longer be detected (1). macroH2A1.2 is also found at pericentric heterochromatin in round spermatids with HP1α (2, 11, 40, 43, 54, 61, 62). Loss of *Suv39h* histone methyltransferase inhibits spermatogenesis (47). To date, no study has examined the role or localization of H2A.Z during spermatogenesis.

In the present study, we addressed this question by analyzing the specific nuclear localization of H2A.Z during the key stages of mouse spermatogenesis and its relationship with macroH2A and other repressive marks that define heterochromatin. We show that: (i) H2A.Z is weakly expressed during the early stages of spermatogenesis, but its expression begins to increase at pachytene when MSCI occurs, peaking at the round spermatid stage; (ii) at pachytene dramatic changes also occur in the nuclear localization and appearance of the key determinants that define heterochromatin; and (iii) in postmeiotic round spermatids, the sex chromosomes are assembled into a facultative heterochromatic state and are enriched with H2A.Z. We therefore propose that H2A.Z may have a role in keeping the sex chromosomes in a transcriptionally repressed state.

MATERIALS AND METHODS

Meiotic sections, surface spread preparations, and immunocytochemistry. Meiotic sections (26) and surface spread spermatogenic cells (48) were prepared for immunocytochemistry as previously described. After permeabilization in 1% Triton X-100, slides were blocked in phosphate-buffered saline (PBS) containing 3% bovine serum albumin for 45 min at room temperature and then incubated at 37°C for 45 min with the primary antibody. H2A.Z and H2A were detected by a sheep monoclonal antibody raised against mouse H2A.Z and H2A at dilutions of 1:500 and 1:200, respectively. All acetylated and methylated histone antibodies were supplied from Upstate (1:100 dilution), apart from the H3-K27 trimethylation antibody, which was obtained from Abcam (1:100 dilution). Mouse monoclonal antibodies to HP1 were obtained from Chemicon (1:100 dilution). MacroH2A was detected by using a polyclonal rabbit antibody (kindly supplied by John Pehrson) at a 1:100 dilution. The antibody for the phosphorylated form of RNA polymerase II (serine 2; 1:50) was obtained from Covance. A rabbit polyclonal antibody to the synaptonemal complex protein SCP3 (1:100) was obtained from Abcam. After two washes in PBS, slides were incubated with a secondary antibody for 45 min at 37°C. Secondary antibodies used were fluorescein isothiocyanate (FITC)-conjugated donkey anti-sheep immunoglobulin G (IgG; Jackson), indocarbocyanine (Cy3)-conjugated donkey anti-sheep IgG (Jackson), FITC-conjugated donkey anti-rabbit IgG (Jackson), and FITC-conjugated donkey anti-mouse IgG (Jackson). Slides were subsequently washed twice in PBS and counterstained with DAPI (4′,6′-diamidino-2-phenylindole) or propidium iodide. Slides were mounted with Vectorshield anti-fade mounting media (Vector).

To quantitatively determine changes in H2A.Z protein levels during spermatogenesis, one standard exposure time was used to measure the amount of fluorescence (and one for DAPI staining) in germ cells at different stages of spermatogenesis (identified by anti-SCP3 staining). The mean intensity of at least 10 cells for each spermatogenic stage was determined by using Image Pro-plus 5.1. To take into account changes of fluorescence intensity due to chromatin compaction, the mean ratio of H2A.Z fluorescence to DAPI staining was determined.

Quantitative RT-PCR. RNA was isolated from various stages of spermatogenesis as previously described (56). Reverse transcription (RT) with random decamer primers was performed with the RETROScript RT Kit (Ambion) after treatment of 1 μg of purified RNA with TURBO DNase (Ambion). The resulting cDNAs were used as templates for PCR with the following gene-specific primers: APRT, 5′-CCAGCAGCACTAGGAACTGCTT and 5′-AGGGTGTG TGGGACGTGTACAA; ZFY, 5′-AAGATAAGCTTACATAATCACATGGA and 5′-CCTATGAAATCCTTTGCTGCACATGT; H2A.Z, 5′-CCAAGACAA AGGCGGTTTCC and 5′-TCCTGCCAACTCAAGTACCTC; and GAPDH, 5′-GTGAAGGTCGGTGTGAACGGAT and 5′-CTGGAAGATGGTGATGGGC TTC. Real-time RT-PCR was performed by using the SYBR Green PCR master mix and the 7900 Thermal cycler at typical amplification parameters (50°C for 2 min and 95°C for 10 min, followed by 40 cycles of 95°C for 15 s and 60°C for 1 min), and the fold differences were determined by comparing the ΔC_T value of each gene normalized with GAPDH using REST-2 software.

FISH. Fluorescence in situ hybridization (FISH) was carried out as previously described (20). Briefly, meiotic cells were fixed in methanol-acetic acid (3:1), denatured at 70°C for 2.5 min, and then washed with cold ethanol (70 to 90% [vol/vol]). X and Y chromosome paints (Cambio) labeled with FITC and CY3, respectively, were denatured at 70°C for 6 min, along with 1 μg of mouse COT1-DNA (Invitrogen). After re-annealing for 20 min at 37°C, the paints were hybridized to the sex chromosomes overnight at 37°C. Slides were then washed three times in 50% formamide–1× SSC (1× SSC is 0.15 M NaCl plus 0.015 M sodium citrate), and once in 2× SSC at 40°C. Cells were stained with DAPI (Sigma) before being mounted with Vectorshield.

Microscopy. Samples were observed with a Leica confocal fluorescence or an Olympus I × 70 microscope. Digital images and signal intensity charts were prepared by using Image-Pro Plus (Media Cybernetics), Microsoft Excel, and Adobe Photoshop 7.0 software.

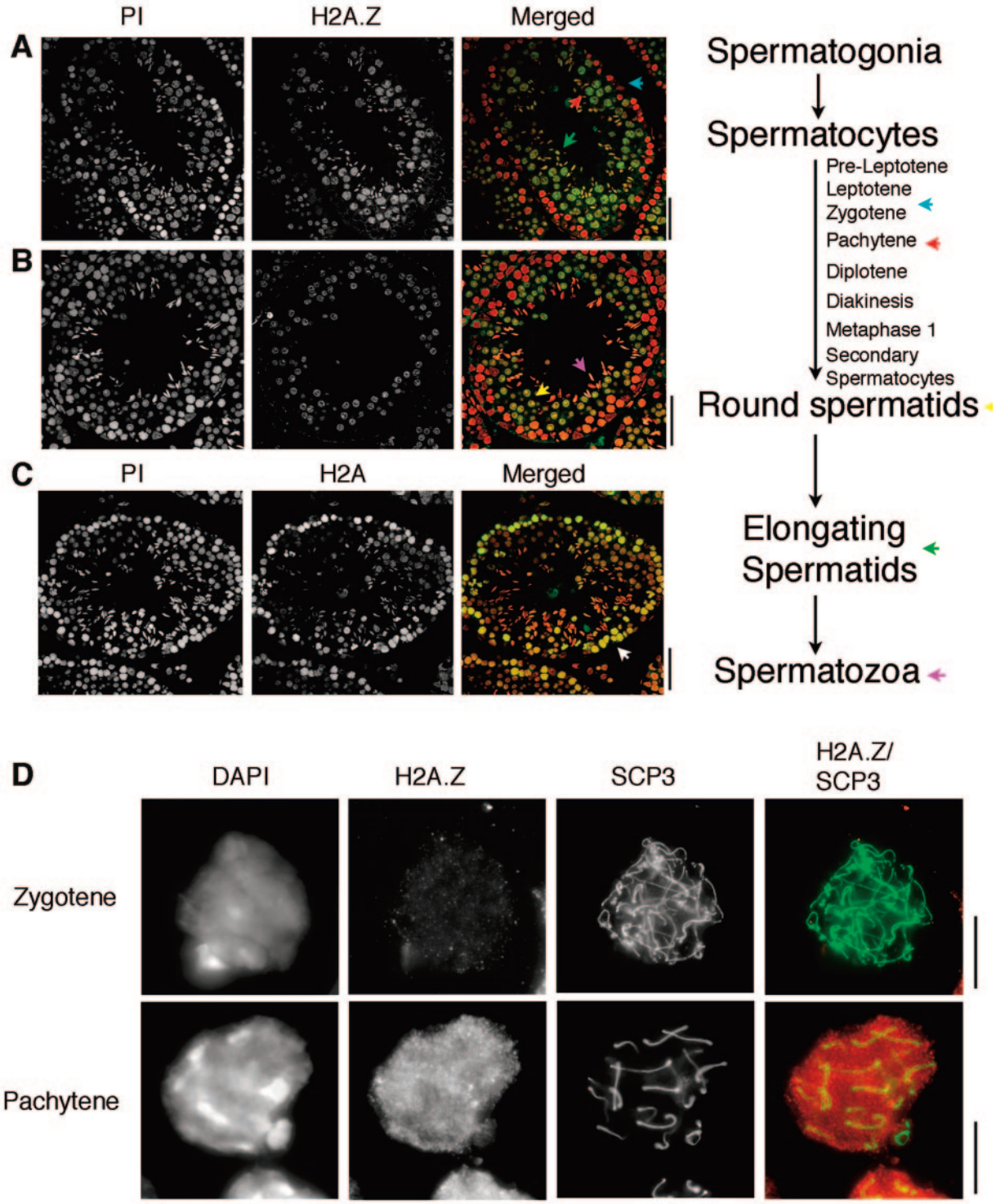

FIG. 1. H2A.Z is first observed at the pachytene cell stage. Mouse seminiferous tubules were stained with propidium iodide (PI) and immunostained with H2A.Z (A and B) or H2A (C) affinity-purified antibodies. For the merged panel, the first and second panels are artificially colored red and green, respectively. Bar, 50 μm. (D) To determine at which stage of meiotic prophase H2A.Z becomes apparent, meiotic surface spread spermatocytes were stained with an H2A.Z antibody (red) and an antibody to the synaptonemal complex marker SCP3 (green). Also shown is an outline highlighting the basic steps during spermatogenesis. Colored arrows highlighting the different cell types are shown and used in the merged panel to illustrate the location of the major cell types in the seminiferous tubule. Bar, 10 μm.

RESULTS

H2A.Z expression increases at pachytene and peaks in round spermatids. In mammals, spermatogenesis occurs in the seminiferous tubule. Stem cell spermatogonia are located at the outer edge of these tubes (44). Some spermatogonia stop proliferating and differentiate into primary spermatocytes, which enter the first meiotic prophase. The first meiotic prophase can be divided into five sequential stages (leptotene, zygotene, pachytene, diplotene, and diakinesis; see Fig. 1) (44, 57). During these stages, major chromosomal structural changes occur as they undergo synapsis, recombination, and desynapsis (6). Cells then continue with division I of meiosis to produce secondary spermatocytes, which then undergo meiotic division II to produce haploid round spermatids. Differentiation continues to proceed toward the center of the tubule that ultimately yields mature spermatozoa, which escape into the lumen.

To investigate the distribution and nuclear localization of H2A.Z during spermatogenesis, we indirectly immunofluorescently labeled mouse testis sections with affinity-purified H2A.Z (Fig. 1A and B) and H2A antibodies (Fig. 1C). There was little H2A.Z in leptotene-to-zygotene (leptotene/zygotene) meiotic cells (Fig. 1A, blue arrow), or at earlier stages (data not shown, Fig. 2A). H2A.Z is first observed in pachytene spermatocytes (Fig. 1A, red arrow). H2A.Z was also detected in round spermatids (Fig. 1B, yellow arrow) and persisted into stage 11-12 elongating spermatids (Fig. 1A, green arrow) at a time when global transcription is shut down (30). H2A.Z could not be detected in spermatozoa (Fig. 1B, purple arrow), although trace amounts were previously detected in human sperm by a biochemical approach (18).

The H2A.Z immunolocalization patterns of mouse spermatogenic sections were then compared to sections immunostained with H2A affinity-purified antibodies. Both antibodies were raised against the C terminus, where the major differences between H2A and H2A.Z exist (50). H2A was detected throughout spermatogenesis but was most enriched in leptotene/zygotene meiotic cells (Fig. 1C, white arrow). The intensity of H2A fluorescence then declines just as H2A.Z appears in pachytene spermatocytes.

To confirm that H2A.Z first becomes apparent at pachytene, surface spread preparations of testis were labeled with H2A.Z antibodies, as well as an antibody that recognizes the synaptonemal complex protein SCP3 (Fig. 1D). Pachytene is recognized as the stage at which a fully complete synaptonemal complex is assembled (Fig. 1D) and is the time when inactivation of the X and Y chromosome occurs, forming the sex vesicle (Fig. 3) (26, 27, 29). Although there was little H2A.Z in leptotene/zygotene cells, a significant increase in H2A.Z occurred at pachytene being spread throughout the nucleus. H2A.Z is present but not concentrated at pericentric heterochromatin (identified by intense DAPI staining at distinct foci) (Fig. 1D), as observed in several mammalian cell lines (51; Greaves and Tremethick, unpublished).

To quantitatively determine the changes in H2A.Z protein levels throughout spermatogenesis, the amount of fluorescence in germ cells at different stages of spermatogenesis (identified by anti-SCP3 staining [data not shown]) was quantitated (see Materials and Methods). To take into account changes of fluorescence intensity due to chromatin compaction, the mean ratio of H2A.Z fluorescence to DAPI staining was determined and plotted (Fig. 2A). Strikingly, while the level of H2A.Z began to increase at pachytene, the maximum level of H2A.Z protein occurred in round spermatids. Round spermatids are the haploid products of the meiosis process. The potential significance of this finding is discussed below (see Fig. 8).

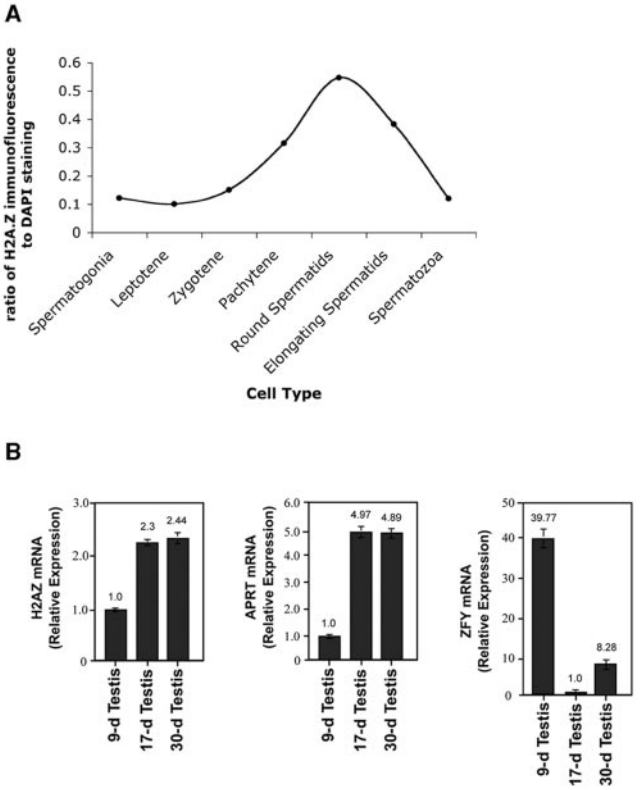

FIG. 2. H2A.Z protein expression peaks at the round spermatid stage. (A) The amount of indirect fluorescence generated by affinity-purified H2A.Z antibodies was determined and quantitated for germ cells at different stages of spermatogenesis, as described in Materials and Methods. To take into account changes in fluorescence intensity due to chromatin compaction, the mean ratio of H2A.Z fluorescence to DAPI staining was determined. (B) Transcript levels of H2A.Z, adenine phosphoribosyltransferase (APRT), and Y-linked zinc finger protein (ZFY) from 9-, 17-, and 30-day-old mice were determined by quantitative real-time PCR using glyceraldehyde phosphate dehydrogenase as an internal control.

To correlate this increase in H2A.Z at pachytene with its transcript levels, RNA was extracted from germ cells at various stages of spermatogenesis (9-, 17-, and 30-day-old mice) (Fig. 2B). Consistent with the immunostaining data, the H2A.Z transcripts are 2.3-fold higher in pachytene spermatocytes (day 17) compared to spermatogonia cells (day 9). H2A.Z transcript levels were also determined with 30-day-old mice, which comprised a mixture germ cells up to the extended spermatid stage; the level of H2A.Z transcript was 2.4-fold higher than in spermatogonia cells. Previously, it was reported that the transcript level of adenine phosphoribosyltransferase was ~5-fold higher in pachytene cells compared to spermatogonia cells. Conversely, the Y-linked zinc finger protein (ZFY) transcript level was ~5-fold higher in spermatogonia cells (56). As a control,

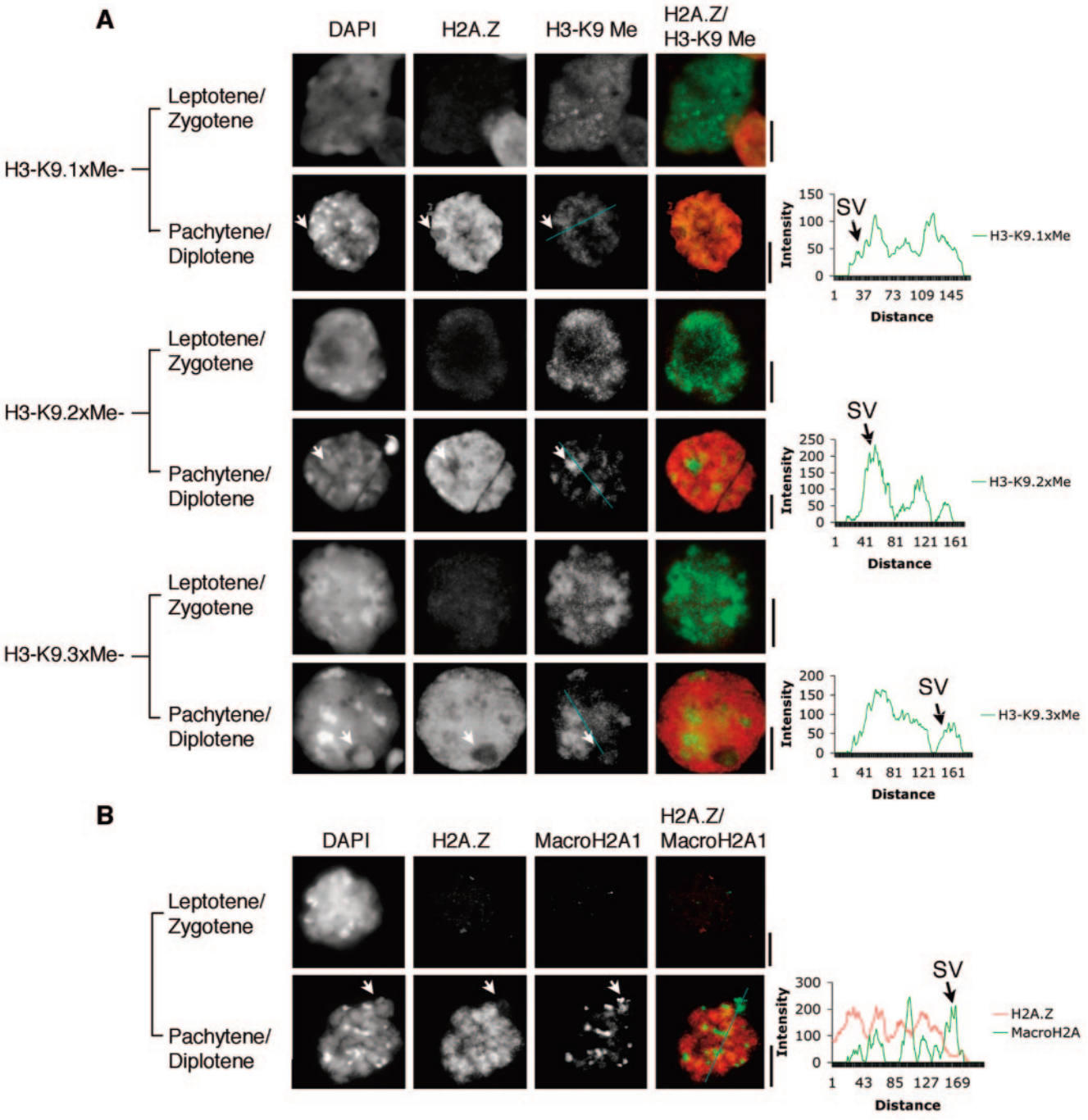

FIG. 3. Dynamic nuclear relocalization of di- and trimethylated H3 K9 when H2A.Z appears at pachytene/diplotene. Surface spread leptotene/zygotene and pachytene cells were stained with DAPI and immunostained with H2A.Z and H3 methylated K9 antibodies (A) or macroH2A antibodies (B) as shown. For the merged panel, the second and third panels are artificially colored red and green, respectively. White arrows indicate the location of the sex vesicle (SV). Shown are the paths used to determine fluorescence intensity in pachytene/diplotene nuclei. Bar, 10 μm. The scales are in arbitrary units.

utilizing the same RNA samples as used for our H2A.Z transcript analysis, we confirmed the findings by these authors (56), thus supporting our conclusion (Fig. 2B).

We conclude that (i) H2A.Z expression is regulated in a differentiation-specific manner with a significant increase in expression at pachytene with the peak of protein expression occurring in the round spermatid stage and (ii) H2A.Z levels are not correlated with the transcription process since its protein expression is low during the earliest stages of spermatogenesis when transcription rates are high (63, 65).

Dynamic nuclear relocalization of heterochromatic marks at pachytene. To study the interplay between H2A.Z and post-

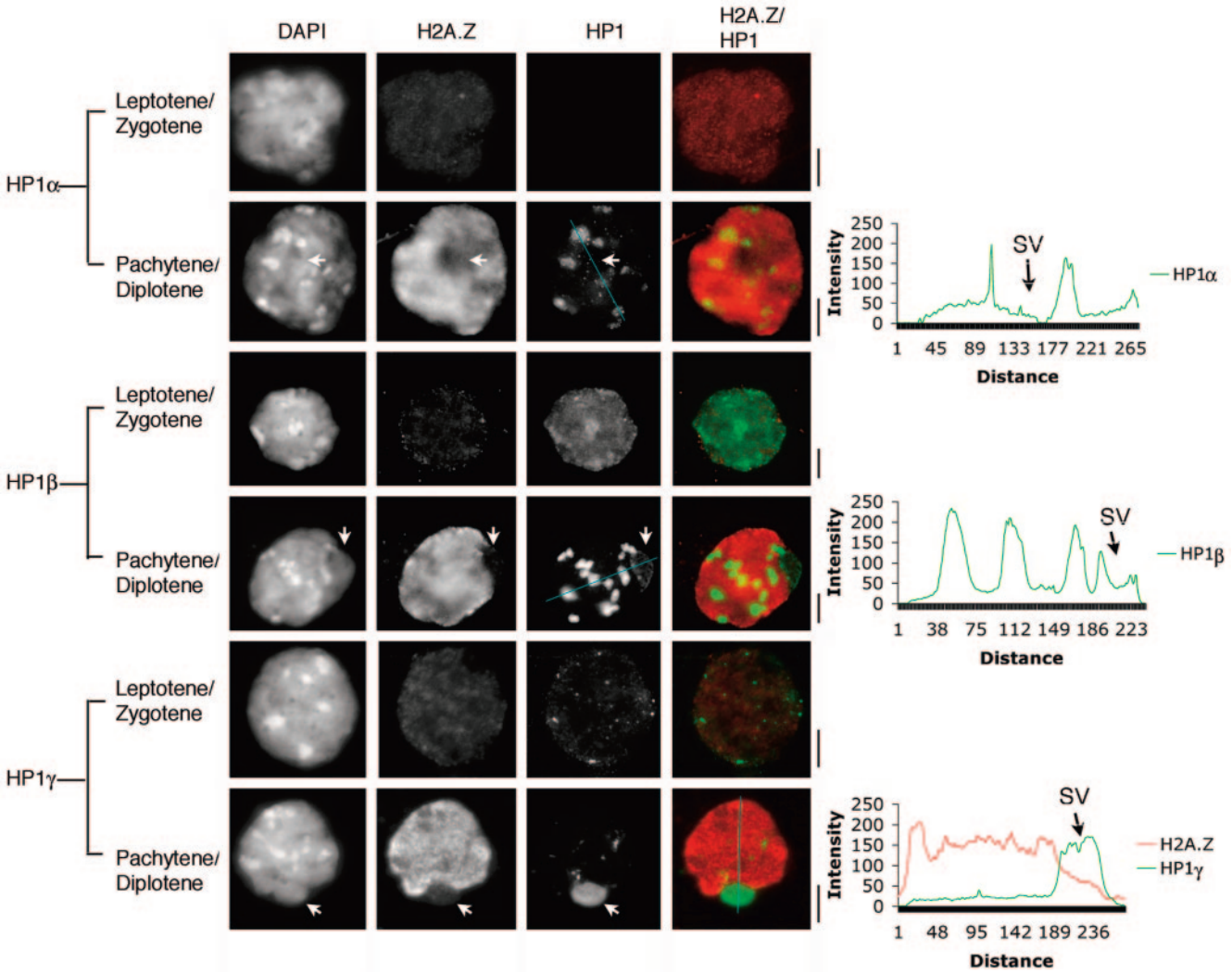

FIG. 4. HP1α and -β accumulate in constitutive heterochromatic domains at pachytene/diplotene. Surface spread leptotene/zygotene and pachytene cells were stained with DAPI and immunostained with H2A.Z, as well as HP1α, HP1β, or HP1γ antibodies, as shown. For the merged panel, the second and third panels are artificially colored red and green, respectively. White arrows show the location of the sex vesicle (SV). Shown are the paths used to determine fluorescence intensity in pachytene/diplotene nuclei. Bar, 10 μm.

translational modifications associated with heterochromatin formation around pachytene, immunofluorescence experiments were performed using surface spreads with antibodies against histone modifications associated with constitutive (H3-K9 trimethylation and K27 monomethylation) and facultative (H3-K9 dimethylation and H3-K27 trimethylation) heterochromatin (Fig. 3A and 5, respectively). The appearance and localization of macroH2A (Fig. 3B) and different HP1 family members (Fig. 4) were also investigated. Given that it was not possible to carry out triple-immunostaining experiments (using SCP3 as the third antibody), we could not unambiguously distinguish between pachytene and diplotene spermatocytes.

Interestingly, leptotene/zygotene cells (Fig. 3A) contained H3-K9 di- and trimethylation not only at DAPI foci (constitutive heterochromatin) but also distributed throughout the whole nucleus. Strikingly, trimethylated H3-K9 and dimethylated K9 dynamically relocates and concentrates at pericentric heterochromatin at pachytene/diplotene when H2A.Z is present. The appearance of the facultative XY sex vesicle (white arrow) at pachytene/diplotene can also be clearly observed. Although H3-K9 trimethylation is not excluded, the sex vesicle also became enriched with dimethylated H3-K9 (Fig. 3A) and macroH2A but not with H2A.Z (Fig. 3B). To show this more clearly, we quantitated and plotted the intensity of the fluorescence signals generated by these different antibodies following the shown paths across the sex vesicle and the remainder of the pachytene/diplotene nucleus.

Consistent with this concentration of methylated H3 at heterochromatic domains, HP1β also relocates to pericentric heterochromatin and the sex vesicle at pachytene/diplotene (Fig. 4) as reported previously (61). Interestingly, HP1α could not be detected in leptotene/zygotene cells, but strong immunofluorescent foci appeared at pachytene/diplotene in constitutive heterochromatic domains but not at the sex vesicle. As expected HP1γ, became highly enriched at the sex vesicle (Fig. 4) (40) at a time when H2AX becomes phosphorylated (16, 60).

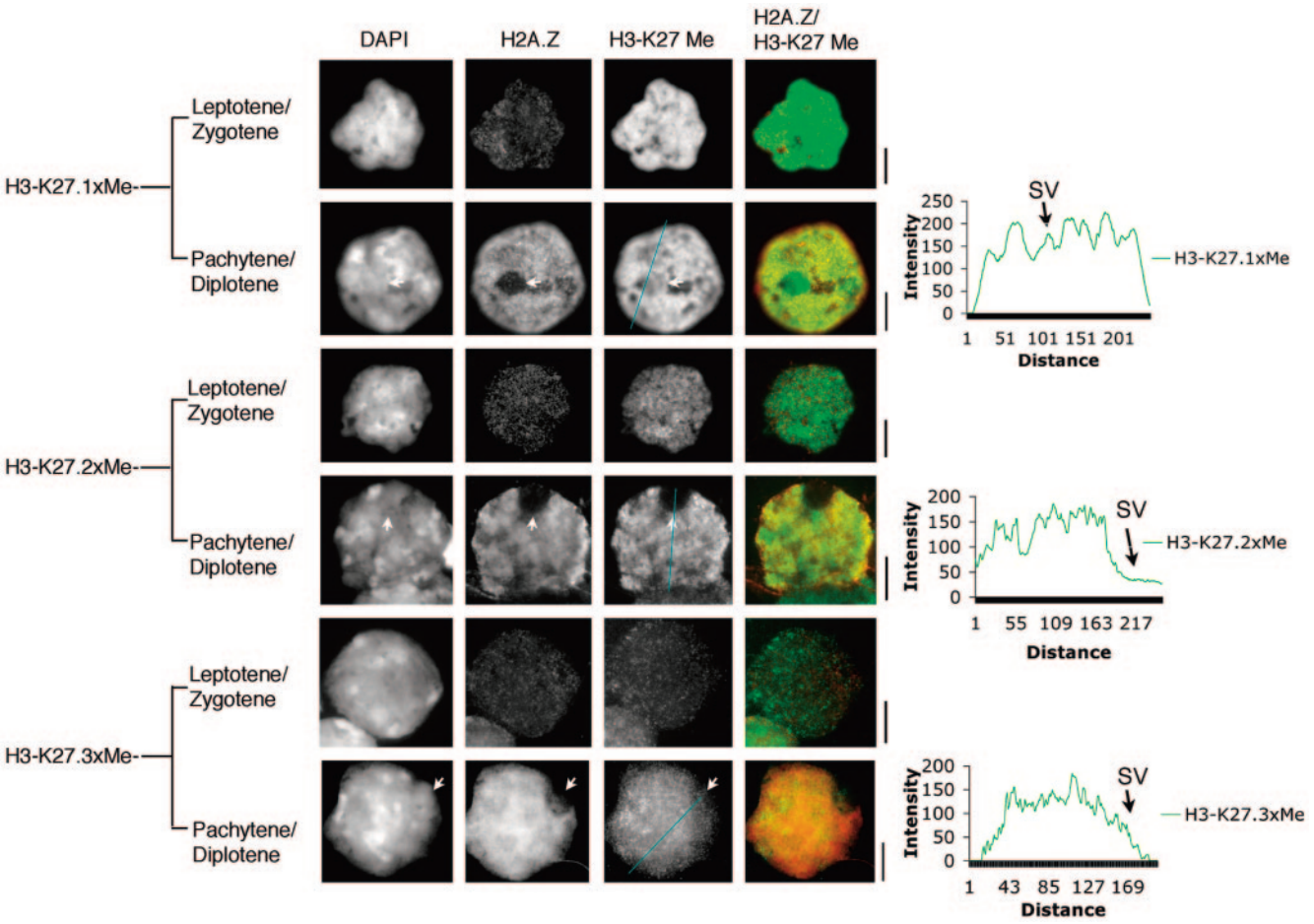

FIG. 5. Enrichment of histone H3 tri-methyl K27 at pachytene/diplotene. Surface spread leptotene/zygotene and pachytene cells were stained with DAPI and immunostained with H2A.Z and histone H3 methylated K27 antibodies as shown. For the merged panel, the second and third panels are artificially colored red and green, respectively. White arrows show the location of the sex vesicle (SV). Shown are the paths used to determine fluorescence intensity in pachytene/diplotene nuclei. Bar, 10 μm.

The most significant change in H3 lysine 27 methylation is a marked increase in the level of H3 K27 trimethylation from leptotene/zygotene to pachytene/diplotene (Fig. 5). Although nuclear staining patterns are not uniform, there appears to be no specific enrichment of H3 methylated at K27 (mono-, di-, or trimethylated) at pericentric heterochromatin. Only dimethylated H3 K27 is excluded from the sex vesicle.

We conclude that in addition to the appearance of H2A.Z, other major dynamic changes in the composition and architecture of chromatin occur at pachytene/diplotene. We found that (i) di- and trimethylated H3 K9 and HP1β relocate to concentrate at domains of heterochromatin; (ii) macroH2A, HP1α, and trimethylated H3 K27 accumulate in the nucleus with H2A.Z; and (iii) constitutive and facultative heterochromatin can share the same marks.

H2A.Z accumulates on the sex chromosomes postmeiotically. Major changes in nuclear organization and chromatin conformation continue upon the completion of meiosis. In late round spermatids, the haploid products of meiosis, mouse chromosomes occupy distinct territories so that pericentric heterochromatin from all chromosomes aligns and accumulates in the center of the round spermatid, forming a large single chromocenter (41, 66). Centromeres are located within this central structure, whereas telomeres are found at the nuclear periphery. As reported in Fig. 2A, H2A.Z protein expression is maximal at this stage. Further differentiation results in the elongation of round spermatids and the compaction of the genome by replacement of histones with transitional proteins and then protamines, leading ultimately to the formation of mature spermatozoa (45).

Figure 6A shows the nuclear localization of H2A.Z and specific methylated lysine forms of H3 in round and elongated spermatids. As expected, round spermatids contain a single large heterochromatic chromocenter enriched with H3 trimethylated K9. The intensity of the fluorescence signal generated by this, and all other antibodies, was quantitated and plotted following the shown path across the round spermatid nucleus. The fluorescence intensity of tri-K9 H3 methylation follows the concentration of DNA (as indicated by DAPI staining), clearly peaking at the chromocenter.

Interestingly, immediately adjacent to the chromocenter is a large distinct region that also stains brightly with DAPI (white arrows), indicating that it is also an area of compacted chromatin. Significantly, this nuclear domain is selectively enriched

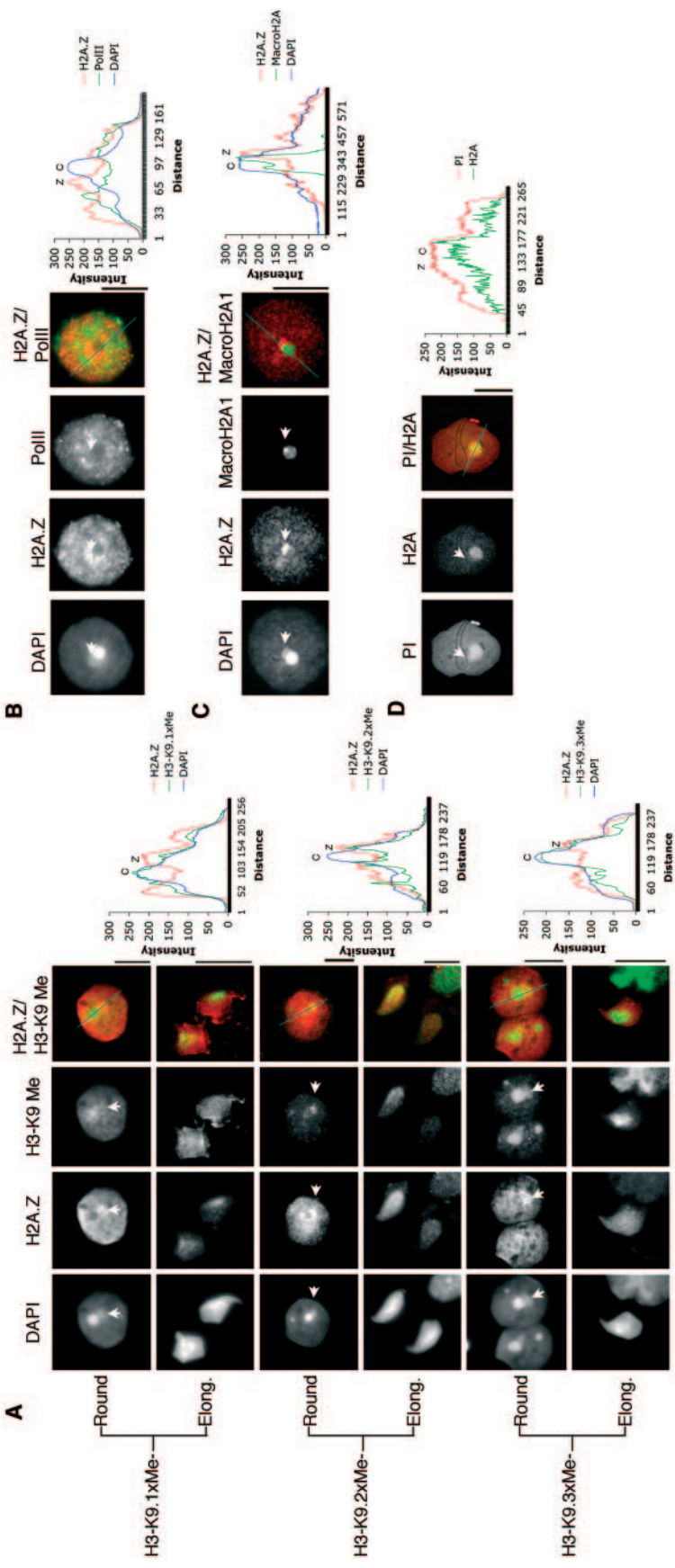

FIG. 6. A unique chromosomal domain enriched H2A.Z. (A) Surface spread round and elongated spermatid cells were stained with DAPI and immunostained with H2A.Z (red) and histone H3 methylated K9 antibodies (green) as shown. (B) Round spermatids immunostained with antibodies against H2A.Z (red) and a phosphorylated form of RNA polymerase II (green). (C) Round spermatids were stained with DAPI and immunostained with H2A.Z (red) and macroH2A (green) antibodies. (D) Round spermatids were stained with propidium iodide (red) and immunostained with H2A (green) antibodies. White arrows show the location of the H2A.Z enriched domain. Shown are the paths used to determine fluorescence intensity in round spermatid nuclei. C, chromocenter; Z, the enriched H2A.Z domain next to the chromocenter. Bar, 10 μm.

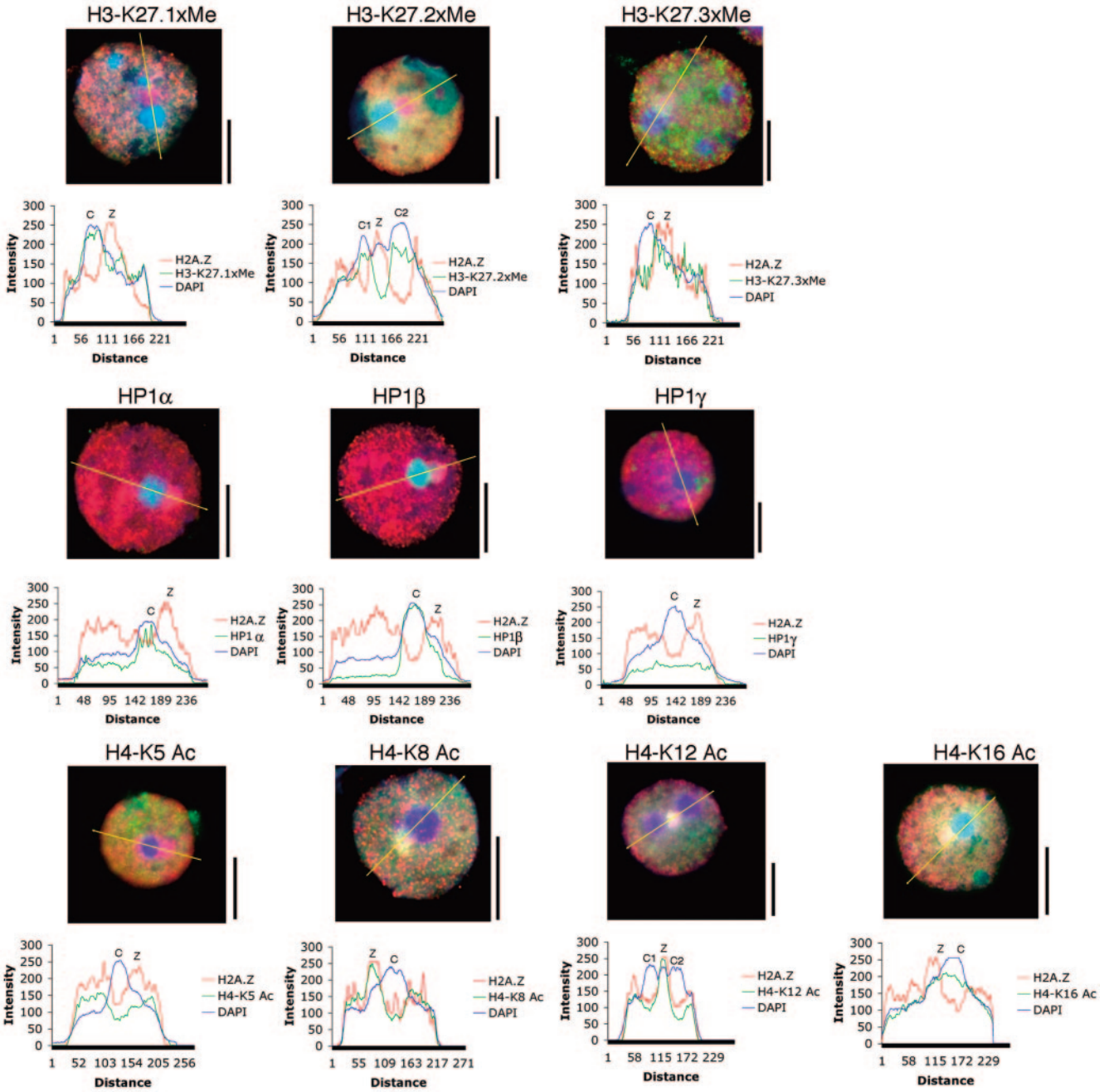

FIG. 7. Histone modification status of the distinct H2A.Z chromosomal domain. Round spermatids were immunostained with a battery of different antibodies as shown. The intensity of fluorescence for each antibody following a linear path across the nucleus are shown and plotted. C, chromocenter; Z, the enriched H2A.Z domain next to the chromocenter. Bar, 10 μm.

with H2A.Z and dimethylated H3 K9 (Fig. 6A) and depleted in the active form of RNA polymerase II (Fig. 6B), macroH2A (Fig. 6C), and H2A (Fig. 6D).

To further characterize this H2A.Z/dimethyl K9 H3 containing domain located next to the chromocenter, we determined whether it was associated with H3 methylated at K27 (mono-, di-, or trimethylated), HP1 (α, β, or γ), and/or acetylated H4 (K5, K8, K12, or K16) (Fig. 7). This H2A.Z domain lacks H3 mono- and di-K27 methylation but is enriched with trimethylated H3 K27, a mark of facultative heterochromatin. Like H2A and macroH2A, HP1α and -β are concentrated at the chromocenter, while HP1γ is distributed throughout the whole nucleus at a low level. Interestingly, this domain is also preferentially enriched with H4 acetylated at lysine residues 8 and 12 but not at residue 5 or 16. Most importantly, extensive analysis of round spermatids (n = 120) revealed that this H2A.Z nuclear domain exists in all round spermatids with the same set of histone modifications (data not shown).

Although a minority of genes on the X and Y chromosomes become transcriptionally activated, the bulk of genes remain

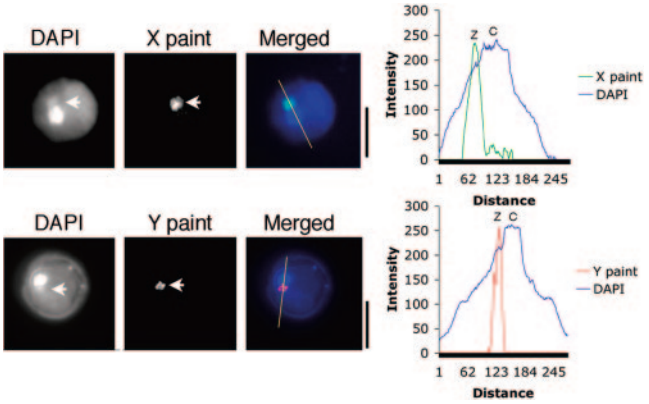

FIG. 8. The unique chromosomal domain enriched with H2A.Z are the sex chromosomes. FISH analyses were performed on round spermatids using specific chromosome X and Y paints. White arrows indicate the location of the H2A.Z enriched domain. Shown are the paths used to determine fluorescence intensity. C, chromocenter; Z, the enriched H2A.Z domain next to the chromocenter. Bar, 10 μm.

transcriptionally repressed following MSCI (29, 52), even though phosphorylated H2A.X (16, 60) and macroH2A (26) disappear. To investigate the possibility that the H2A.Z-containing domain depleted in RNA polymerase II (Fig. 6B) contains a sex chromosome, FISH analyses were performed using specific chromosome X and Y paints. Figure 8 (and data not shown) clearly demonstrates that this nuclear territory enriched with H2A.Z comprises either the X or the Y chromosome in haploid round spermatids. Most interestingly, a study has revealed that while the association of macroH2A1.2 with pericentric heterochromatin is lost on the X chromosome, it persists on the Y chromosome in round spermatids (61). Consistent with this, about half of the round spermatids analyzed ($n = 120$) contained a small foci of macroH2A next to the H2A.Z domain (Fig. 6C).

In elongated spermatids, when global transcription ceases, H2A.Z is found throughout the nucleus (Fig. 5A). At later stages, H2A.Z disappears (Fig. 2) as histones in general are displaced from the mouse genome with transition proteins.

Taken together, we conclude that (i) at the completion of meiosis, when the expression of H2A.Z peaks (Fig. 2), the X and Y chromosomes are assembled into a repressed facultative heterochromatic state enriched with H2A.Z, thus replacing macroH2A; (ii) this facultative heterochromatin comprises modifications that define both inactive and active chromatin; (iii) the X and Y chromosomes share the same histone modification status; and (iv) the sex chromosome (X or Y) occupy a distinct nuclear territory next to the chromocenter in round spermatids.

DISCUSSION

In this study we have used mouse spermatogenesis as a model system to investigate the alterations in nuclear and heterochromatin composition during differentiation. The advantage of this system is that it is possible to monitor the differentiation process from the beginning (spermatogonia) to the end (spermatozoa), enabling the major temporal changes in nuclear and chromatin organization to be analyzed. Using this model system, we have analyzed the role of H2A.Z and its interplay with other components of heterochromatin. We show that large-scale nuclear alterations and continuous changes to heterochromatin accompany the differentiation process. Key components of facultative and constitutive heterochromatin relocate and appear at important stages during mouse spermatogenesis. Significantly, we demonstrate that after MSCI the sex chromosomes are assembled into facultative heterochromatin enriched with H2A.Z, at the time when the expression of H2A.Z protein is at its highest.

Changes in H2A.Z expression mark different stages of spermatogenesis. H2A.Z is expressed at a low level during the early stages of spermatogenesis, and this low expression continues until the first meiotic prophase, at pachytene, when MSCI occurs (see below). Strikingly, the level of H2A.Z protein then dramatically increases, peaking at the round spermatid stage. H2A.Z can be detected in elongated spermatids, when transcription ceases, and disappears after this stage. Interestingly, H2A.Z also appears at meiotic prophase in micronuclei of *Tetrahymena* (which serve as the germ line) (58). During this period of low H2A.Z expression prior to pachytene, gene expression is high on autosomes and sex chromosomes (29, 52, 65). This indicates that H2A.Z levels do not correlate with the transcription process.

These observations are consistent with our previous finding that H2A.Z expression is markedly upregulated upon the differentiation of the mouse inner cell mass to specialized cell types being targeted to pericentric heterochromatin (50). We therefore propose that a low level of H2A.Z may be a general feature of the undifferentiated and/or rapidly dividing state and, upon differentiation, the increase in H2A.Z is responsible for changes to the quantity and/or quality of heterochromatin. Further support for this proposal comes from our finding that the X and Y chromosomes are assembled into heterochromatic structures enriched with H2A.Z in round spermatids (see below).

The appearance of H2A.Z at pachytene correlates with other major dynamic changes to the composition and organization of chromatin. In leptotene/zygotene cells, di- and trimethylated H3 K9 and HP1β have a ubiquitous distribution throughout the nucleus. This distribution of heterochromatin marks changes dramatically at pachytene/diplotene in the presence of H2A.Z. Dimethylated H3 K9 and HP1β relocates and concentrates at the pericentric heterochromatin and the sex vesicle, while the general nuclear staining of trimethylated H3 K9 disappears, becoming more intense at chromocenters. Significantly, other components of heterochromatin (macroH2A, HP1α, and trimethylated H3 K27) appear at pachytene/diplotene.

In line with our hypothesis presented above, we suggest that H2A.Z can substitute for H3 K9 methylation and H1β in euchromatin, enabling these marks to relocate and concentrate at the XY body and pericentric heterochromatin. Similarly, H2A.Z associates with the sex chromosomes to compensate for the loss of macroH2A and phosphorylated H2A.X in round spermatids. Supporting such a proposal, H2A.Z is enriched at the pericentric heterochromatin (50) when trimethylated H3 K9 is depleted (38) in extraembryonic cells. Significantly, inactivation of a lysosomal and nuclear protease, cathepsin L, leads to a dramatic loss of H3 K9 trimethylation at the pericentric heterochromatin and the Y chromosome in mouse fi-

broblasts, leading to a global repositioning of H2A.Z to these heterochromatic domains to replace trimethylated H3 K9 (4) to maintain proper chromosome function. Clearly, complex universal mechanisms operate to maintain and regulate heterochromatin structure and function.

A major finding of the present study is that, in addition to macroH2A and phosphorylated H2A.X, H2A.Z not only associates with the X chromosome but also with the Y chromosome. Whereas macroH2A participates in the silencing of the sex chromosomes at MSCI, we suggest that H2A.Z maintains this silenced state postmeiotically in round spermatids by directly facilitating the compaction of the chromatin fiber (14, 15). This is consistent with our observation that RNA polymerase II is depleted on sex chromosomes (which stain brightly with DAPI and therefore are still compacted) in round spermatids. Although a minority of genes on the X and Y are reactivated after meiosis (25, 39), net transcription from both sex chromosomes decreases dramatically at MSCI, and this low expression is maintained postmeiotically (29). Evolutionary pressures have evidently ensured that genes expressed after MSCI are prohibited from residing on the X chromosome (52). Our findings also demonstrate that, like macroH2A, H2A.Z can participate in the assembly of both constitutive (50) and facultative heterochromatin. However, compared to macroH2A, perhaps H2A.Z assembles compacted heterochromatic structures that are less refractory to transcription (14).

It is also possible that H2A.Z has other roles. Since "heterochromatin likes heterochromatin," the enrichment of the sex chromosomes with H2A.Z may help localize these chromosomes next to the chromocenter. The position of chromosomes in sperm is highly ordered (20), and it has been argued that this positioning may exert a level of control on the order in which chromosomal domains are decompacted and expressed after fertilization (36).

We observe that the X and Y chromosomes share the same profile of histone modifications in round spermatids comprising the facultative marks trimethylated H3 K27 and dimethylated H3 K9 and, interestingly, the active acetylated H4 mark (lysine residues 8 and 12). H4 is also acetylated in the XY body at meiosis (2). A recent study interpreted this acetylation of H4 in round spermatids as being required for the transcriptional activation of the X chromosome (28). However, since most genes on the mouse X chromosome are inactive following MSCI, this global acetylation may have other functions. It may facilitate the replacement of macroH2A and H2A with H2A.Z after MSCI and the subsequent global replacement of histones with transition proteins in elongated spermatids. It is worth noting that *Drosophila* constitutive heterochromatin is enriched with H4 acetylated at lysine 12 (59).

Finally, since trace amounts of histone H2A.Z have been detected in mammalian sperm using a biochemical approach (18), a speculative proposal is that H2A.Z remains on the X chromosome to provide an epigenetic mark for subsequent paternal X inactivation during mouse embryogenesis. In conclusion, the present study provides new insights into the dynamic chromatin changes associated with spermatogenesis and a new role for H2A.Z in the structure and function of sex chromosomes.

ACKNOWLEDGMENTS

We thank Pat Ridgway for critically reading the manuscript.

This study was supported by an NHMRC grant to D.R. and D.J.T.

REFERENCES

1. **Abbott, D. W., M. Laszczak, J. D. Lewis, H. Su, S. C. Moore, M. Hills, S. Dimitrov, and J. Ausio.** 2004. Structural characterization of macroH2A containing chromatin. Biochemistry **43:**1352–1359.
2. **Armstrong, S. J., M. A. Hulten, A. M. Keohane, and B. M. Turner.** 1997. Different strategies of X-inactivation in germinal and somatic cells: histone H4 underacetylation does not mark the inactive X chromosome in the mouse male germline. Exp. Cell Res. **230:**399–402.
3. **Bruce, K., F. A. Myers, E. Mantouvalou, P. Lefevre, I. Greaves, C. Bonifer, D. J. Tremethick, A. W. Thorne, and C. Crane-Robinson.** 2005. The replacement histone H2A.Z in a hyperacetylated form is a feature of active genes in the chicken. Nucleic Acids Res. **33:**5633–5639.
4. **Bulynko, Y., L. C. Hsing, R. W. Mason, D. J. Tremethick, and S. A. Grigoryev.** 2006. Cathepsin L stabilizes histone modification landscape on Y chromosome and pericentric heterochromatin. Mol. Cell. Biol. **26:**4172–4184.
5. **Byrne, J. A., S. Simonsson, P. S. Western, and J. B. Gurdon.** 2003. Nuclei of adult mammalian somatic cells are directly reprogrammed to oct-4 stem cell gene expression by amphibian oocytes. Curr. Biol. **13:**1206–1213.
6. **Champion, M. D., and R. S. Hawley.** 2002. Playing for half the deck: the molecular biology of meiosis. Nat. Med. **8**(Suppl.)**:**S50–S56.
7. **Churikov, D., J. Siino, M. Svetlova, K. Zhang, A. Gineitis, E. Morton Bradbury, and A. Zalensky.** 2004. Novel human testis-specific histone H2B encoded by the interrupted gene on the X chromosome. Genomics **84:**745–756.
8. **Churikov, D., I. A. Zalenskaya, and A. O. Zalensky.** 2004. Male germline-specific histones in mouse and man. Cytogenet. Genome Res. **105:**203–214.
9. **Costanzi, C., and J. R. Pehrson.** 1998. Histone macroH2A1 is concentrated in the inactive X chromosome of female mammals. Nature **393:**599–601.
10. **Costanzi, C., P. Stein, D. M. Worrad, R. M. Schultz, and J. R. Pehrson.** 2000. Histone macroH2A1 is concentrated in the inactive X chromosome of female preimplantation mouse embryos. Development **127:**2283–2289.
11. **Cowell, I. G., R. Aucott, S. K. Mahadevaiah, P. S. Burgoyne, N. Huskisson, S. Bongiorni, G. Prantera, L. Fanti, S. Pimpinelli, R. Wu, D. M. Gilbert, W. Shi, R. Fundele, H. Morrison, P. Jeppesen, and P. B. Singh.** 2002. Heterochromatin, HP1, and methylation at lysine 9 of histone H3 in animals. Chromosoma **111:**22–36.
12. **Echeverri, K., and E. M. Tanaka.** 2002. Mechanisms of muscle dedifferentiation during regeneration. Semin. Cell Dev. Biol. **13:**353–360.
13. **Faast, R., V. Thonglairoam, T. C. Schulz, J. Beall, J. R. Wells, H. Taylor, K. Matthaei, P. D. Rathjen, D. J. Tremethick, and I. Lyons.** 2001. Histone variant H2A.Z is required for early mammalian development. Curr. Biol. **11:**1183–1187.
14. **Fan, J. Y., F. Gordon, K. Luger, J. C. Hansen, and D. J. Tremethick.** 2002. The essential histone variant H2A.Z regulates the equilibrium between different chromatin conformational states. Nat. Struct. Biol. **9:**172–176.
15. **Fan, J. Y., D. Rangasamy, K. Luger, and D. J. Tremethick.** 2004. H2A.Z alters the nucleosome surface to promote HP1α-mediated chromatin fiber folding. Mol. Cell **16:**655–661.
16. **Fernandez-Capetillo, O., S. K. Mahadevaiah, A. Celeste, P. J. Romanienko, R. D. Camerini-Otero, W. M. Bonner, K. Manova, P. Burgoyne, and A. Nussenzweig.** 2003. H2AX is required for chromatin remodeling and inactivation of sex chromosomes in male mouse meiosis. Dev. Cell **4:**497–508.
17. **Francastel, C., D. Schubeler, D. I. Martin, and M. Groudine.** 2000. Nuclear compartmentalization and gene activity. Nat. Rev. Mol. Cell. Biol. **1:**137–143.
18. **Gatewood, J. M., G. R. Cook, R. Balhorn, C. W. Schmid, and E. M. Bradbury.** 1990. Isolation of four core histones from human sperm chromatin representing a minor subset of somatic histones. J. Biol. Chem. **265:**20662–20666.
19. **Govin, J., C. Caron, C. Lestrat, S. Rousseaux, and S. Khochbin.** 2004. The role of histones in chromatin remodeling during mammalian spermiogenesis. Eur. J. Biochem. **271:**3459–3469.
20. **Greaves, I. K., M. Svartman, M. Wakefield, D. Taggart, A. De Leo, M. A. Ferguson-Smith, W. Rens, P. C. O'Brien, L. Voullaire, M. Westerman, and J. A. Graves.** 2001. Chromosomal painting detects non-random chromosome arrangement in dasyurid marsupial sperm. Chromosome Res. **9:**251–259.
21. **Grigoryev, S. A., T. Nikitina, J. R. Pehrson, P. B. Singh, and C. L. Woodcock.** 2004. Dynamic relocation of epigenetic chromatin markers reveals an active role of constitutive heterochromatin in the transition from proliferation to quiescence. J. Cell Sci. **117:**6153–6162.
22. **Guillemette, B., A. R. Bataille, N. Gevry, M. Adam, M. Blanchette, F. Robert, and L. Gaudreau.** 2005. Variant histone H2A.Z is globally localized to the promoters of inactive yeast genes and regulates nucleosome positioning. PLoS Biol. **3:**e384.
23. **Gurdon, J. B., J. A. Byrne, and S. Simonsson.** 2003. Nuclear reprogramming and stem cell creation. Proc. Natl. Acad. Sci. USA **100**(Suppl. 1)**:**11819–11822.
24. **Hazzouri, M., C. Pivot-Pajot, A. K. Faure, Y. Usson, R. Pelletier, B. Sele, S. Khochbin, and S. Rousseaux.** 2000. Regulated hyperacetylation of core

histones during mouse spermatogenesis: involvement of histone deacetylases. Eur. J. Cell Biol. **79:**950–960.
25. **Hendriksen, P. J., J. W. Hoogerbrugge, A. P. Themmen, M. H. Koken, J. H. Hoeijmakers, B. A. Oostra, T. van der Lende, and J. A. Grootegoed.** 1995. Postmeiotic transcription of X and Y chromosomal genes during spermatogenesis in the mouse. Dev. Biol. **170:**730–733.
26. **Hoyer-Fender, S., C. Costanzi, and J. R. Pehrson.** 2000. Histone macroH2A1.2 is concentrated in the XY-body by the early pachytene stage of spermatogenesis. Exp. Cell Res. **258:**254–260.
27. **Hoyer-Fender, S., E. Czirr, R. Radde, J. M. Turner, S. K. Mahadevaiah, J. R. Pehrson, and P. S. Burgoyne.** 2004. Localisation of histone macroH2A1.2 to the XY-body is not a response to the presence of asynapsed chromosome axes. J. Cell Sci. **117:**189–198.
28. **Khalil, A. M., F. Z. Boyar, and D. J. Driscoll.** 2004. Dynamic histone modifications mark sex chromosome inactivation and reactivation during mammalian spermatogenesis. Proc. Natl. Acad. Sci. USA **101:**16583–16587.
29. **Khil, P. P., N. A. Smirnova, P. J. Romanienko, and R. D. Camerini-Otero.** 2004. The mouse X chromosome is enriched for sex-biased genes not subject to selection by meiotic sex chromosome inactivation. Nat. Genet. **36:**642–646.
30. **Kierszenbaum, A. L., and L. L. Tres.** 1974. Transcription sites in spread meiotic prophase chromosomes from mouse spermatocytes. J. Cell Biol. **63:**923–935.
31. **Kobor, M. S., S. Venkatasubrahmanyam, M. D. Meneghini, J. W. Gin, J. L. Jennings, A. J. Link, H. D. Madhani, and J. Rine.** 2004. A protein complex containing the conserved Swi2/Snf2-related ATPase Swr1p deposits histone variant H2A.Z into euchromatin. PLoS Biol. **2:**e131.
32. **Krogan, N. J., M. C. Keogh, N. Datta, C. Sawa, O. W. Ryan, H. Ding, R. A. Haw, J. Pootoolal, A. Tong, V. Canadien, D. P. Richards, X. Wu, A. Emili, T. R. Hughes, S. Buratowski, and J. F. Greenblatt.** 2003. A Snf2 family ATPase complex required for recruitment of the histone H2A variant Htz1. Mol. Cell **12:**1565–1576.
33. **Lachner, M., R. J. O'Sullivan, and T. Jenuwein.** 2003. An epigenetic road map for histone lysine methylation. J. Cell Sci. **116:**2117–2124.
34. **Lewis, J. D., D. W. Abbott, and J. Ausio.** 2003. A haploid affair: core histone transitions during spermatogenesis. Biochem. Cell Biol. **81:**131–140.
35. **Li, B., S. G. Pattenden, D. Lee, J. Gutierrez, J. Chen, C. Seidel, J. Gerton, and J. L. Workman.** 2005. Preferential occupancy of histone variant H2AZ at inactive promoters influences local histone modifications and chromatin remodeling. Proc. Natl. Acad. Sci. USA **102:**18385–18390.
36. **Loriot, A., T. Boon, and C. De Smet.** 2003. Five new human cancer-germline genes identified among 12 genes expressed in spermatogonia. Int. J. Cancer **105:**371–376.
37. **Ma, Y., S. B. Jacobs, L. Jackson-Grusby, M. A. Mastrangelo, J. A. Torres-Betancourt, R. Jaenisch, and T. P. Rasmussen.** 2005. DNA CpG hypomethylation induces heterochromatin reorganization involving the histone variant macroH2A. J. Cell Sci. **118:**1607–1616.
38. **Martens, J. H., R. J. O'Sullivan, U. Braunschweig, S. Opravil, M. Radolf, P. Steinlein, and T. Jenuwein.** 2005. The profile of repeat-associated histone lysine methylation states in the mouse epigenome. EMBO J. **24:**800–812.
39. **McCarrey, J. R., C. Watson, J. Atencio, G. C. Ostermeier, Y. Marahrens, R. Jaenisch, and S. A. Krawetz.** 2002. X-chromosome inactivation during spermatogenesis is regulated by an Xist/Tsix-independent mechanism in the mouse. Genesis **34:**257–266.
40. **Metzler-Guillemain, C., J. Luciani, D. Depetris, M. R. Guichaoua, and M. G. Mattei.** 2003. HP1β and HP1γ, but not HP1α, decorate the entire XY body during human male meiosis. Chromosome Res. **11:**73–81.
41. **Meyer-Ficca, M., J. Muller-Navia, and H. Scherthan.** 1998. Clustering of pericentromeres initiates in step 9 of spermiogenesis of the rat (*Rattus norvegicus*) and contributes to a well defined genome architecture in the sperm nucleus. J. Cell Sci. **111:**1363–1370.
42. **Mizuguchi, G., X. Shen, J. Landry, W. H. Wu, S. Sen, and C. Wu.** 2004. ATP-driven exchange of histone H2AZ variant catalyzed by SWR1 chromatin remodeling complex. Science **303:**343–348.
43. **Motzkus, D., P. B. Singh, and S. Hoyer-Fender.** 1999. M31, a murine homolog of *Drosophila* HP1, is concentrated in the XY body during spermatogenesis. Cytogenet. Cell Genet. **86:**83–88.
44. **Oakberg, E. F.** 1956. A description of spermiogenesis in the mouse and its use in analysis of the cell cycle of the seminiferous epithelium and germ cell renewal. Am. J. Anat. **99:**391–413.
45. **Oliva, R., and G. H. Dixon.** 1991. Vertebrate protamine genes and the histone-to-protamine replacement reaction. Prog. Nucleic Acids Res. Mol. Biol. **40:**25–94.
46. **Peters, A. H., S. Kubicek, K. Mechtler, R. J. O'Sullivan, A. A. Derijck, L. Perez-Burgos, A. Kohlmaier, S. Opravil, M. Tachibana, Y. Shinkai, J. H. Martens, and T. Jenuwein.** 2003. Partitioning and plasticity of repressive histone methylation states in mammalian chromatin. Mol. Cell **12:**1577–1589.
47. **Peters, A. H., D. O'Carroll, H. Scherthan, K. Mechtler, S. Sauer, C. Schofer, K. Weipoltshammer, M. Pagani, M. Lachner, A. Kohlmaier, S. Opravil, M. Doyle, M. Sibilia, and T. Jenuwein.** 2001. Loss of the Suv39h histone methyltransferases impairs mammalian heterochromatin and genome stability. Cell **107:**323–337.
48. **Peters, A. H., A. W. Plug, M. J. van Vugt, and P. de Boer.** 1997. A drying-down technique for the spreading of mammalian meiocytes from the male and female germline. Chromosome Res. **5:**66–68.
49. **Raisner, R. M., P. D. Hartley, M. D. Meneghini, M. Z. Bao, C. L. Liu, S. L. Schreiber, O. J. Rando, and H. D. Madhani.** 2005. Histone variant H2A.Z marks the 5′ ends of both active and inactive genes in euchromatin. Cell **123:**233–248.
50. **Rangasamy, D., L. Berven, P. Ridgway, and D. J. Tremethick.** 2003. Pericentric heterochromatin becomes enriched with H2A.Z during early mammalian development. EMBO J. **22:**1599–1607.
51. **Rangasamy, D., I. Greaves, and D. J. Tremethick.** 2004. RNA interference demonstrates a novel role for H2A.Z in chromosome segregation. Nat. Struct. Mol. Biol. **11:**650–655.
52. **Reinke, V.** 2004. Sex and the genome. Nat. Genet. **36:**548–549.
53. **Rice, J. C., S. D. Briggs, B. Ueberheide, C. M. Barber, J. Shabanowitz, D. F. Hunt, Y. Shinkai, and C. D. Allis.** 2003. Histone methyltransferases direct different degrees of methylation to define distinct chromatin domains. Mol. Cell **12:**1591–1598.
54. **Richler, C., S. K. Dhara, and J. Wahrman.** 2000. Histone macroH2A1.2 is concentrated in the XY compartment of mammalian male meiotic nuclei. Cytogenet. Cell Genet. **89:**118–120.
55. **Ridgway, P., K. D. Brown, D. Rangasamy, U. Svensson, and D. J. Tremethick.** 2004. Unique residues on the H2A.Z containing nucleosome surface are important for *Xenopus laevis* development. J. Biol. Chem. **279:**43815–43820.
56. **Singer-Sam, J., M. O. Robinson, A. R. Bellve, M. I. Simon, and A. D. Riggs.** 1990. Measurement by quantitative PCR of changes in HPRT, PGK-1, PGK-2, APRT, MTase, and Zfy gene transcripts during mouse spermatogenesis. Nucleic Acids Res. **18:**1255–1259.
57. **Solari, A. J.** 1976. The spatial relationship of the X and Y chromosomes during meiotic prophase in mouse spermatocytes. Chromosoma **29:**217–236.
58. **Stargell, L. A., J. Bowen, C. A. Dadd, P. C. Dedon, M. Davis, R. G. Cook, C. D. Allis, and M. A. Gorovsky.** 1993. Temporal and spatial association of histone H2A variant hv1 with transcriptionally competent chromatin during nuclear development in *Tetrahymena thermophila*. Genes Dev. **7:**2641–2651.
59. **Turner, B. M., A. J. Birley, and J. Lavender.** 1992. Histone H4 isoforms acetylated at specific lysine residues define individual chromosomes and chromatin domains in *Drosophila* polytene nuclei. Cell **69:**375–384.
60. **Turner, J. M., O. Aprelikova, X. Xu, R. Wang, S. Kim, G. V. Chandramouli, J. C. Barrett, P. S. Burgoyne, and C. X. Deng.** 2004. BRCA1, histone H2AX phosphorylation, and male meiotic sex chromosome inactivation. Curr. Biol. **14:**2135–2142.
61. **Turner, J. M., P. S. Burgoyne, and P. B. Singh.** 2001. M31 and macroH2A1.2 colocalize at the pseudoautosomal region during mouse meiosis. J. Cell Sci. **114:**3367–3375.
62. **Turner, J. M., S. K. Mahadevaiah, D. J. Elliott, H. J. Garchon, J. R. Pehrson, R. Jaenisch, and P. S. Burgoyne.** 2002. Meiotic sex chromosome inactivation in male mice with targeted disruptions of Xist. J. Cell Sci. **115:**4097–4105.
63. **Turner, J. M., S. K. Mahadevaiah, O. Fernandez-Capetillo, A. Nussenzweig, X. Xu, C. X. Deng, and P. S. Burgoyne.** 2005. Silencing of unsynapsed meiotic chromosomes in the mouse. Nat. Genet. **37:**41–47.
64. **Ueno, M., T. Murase, T. Kibe, N. Ohashi, K. Tomita, Y. Murakami, M. Uritani, T. Ushimaru, and M. Harata.** 2004. Fission yeast Arp6 is required for telomere silencing, but functions independently of Swi6. Nucleic Acids Res. **32:**736–741.
65. **Wang, P. J., J. R. McCarrey, F. Yang, and D. C. Page.** 2001. An abundance of X-linked genes expressed in spermatogonia. Nat. Genet. **27:**422–426.
66. **Zalensky, A. O., J. W. Breneman, I. A. Zalenskaya, B. R. Brinkley, and E. M. Bradbury.** 1993. Organization of centromeres in the decondensed nuclei of mature human sperm. Chromosoma **102:**509–518.
67. **Zhang, H., D. N. Roberts, and B. R. Cairns.** 2005. Genome-wide dynamics of Htz1, a histone H2A variant that poises repressed/basal promoters for activation through histone loss. Cell **123:**219–231.